Journal of Power Sources 196 (2011) 7426–7434

Contents lists available at ScienceDirect

Journal of Power Sources

journal homepage: www.elsevier.com/locate/jpowsour

Tungsten carbide modified high surface area carbon as fuel cell catalyst support

Minhua Shao[a,*], Belabbes Merzougui[a,1], Krista Shoemaker[a], Laura Stolar[a], Lesia Protsailo[a], Zachary J. Mellinger[b], Irene J. Hsu[b], Jingguang G. Chen[b,*]

[a] UTC Power, 195 Governor's Highway, South Windsor, CT 06074, USA
[b] Department of Chemical Engineering, University of Delaware, Newark, DE 19716, USA

ARTICLE INFO

Article history:
Received 7 March 2011
Received in revised form 7 April 2011
Accepted 8 April 2011
Available online 20 April 2011

Keywords:
Fuel cell catalysts
Oxygen reduction reaction
Corrosion
X-ray absorption near edge structure
Activity
Durability

ABSTRACT

Phase pure WC nanoparticles were synthesized on high surface area carbon black (800 $m^2 g^{-1}$) by a temperature programmed reaction (TPR) method. The particle size of WC can be controlled under 30 nm with a relatively high coverage on the carbon surface. The electrochemical testing results demonstrated that the corrosion resistance of carbon black was improved by 2-fold with a surface modification by phase pure WC particles. However, the WC itself showed some dissolution under potential cycling. Based on the X-ray diffraction (XRD) and inductively coupled plasma (ICP) analysis, most of the WC on the surface was lost or transformed to oxides after 5000 potential cycles in the potential range of 0.65–1.2 V. The Pt catalyst supported on WC/C showed a slightly better ORR activity than that of Pt/C, with the Pt activity loss rate for Pt/WC/C being slightly slower compared to that of Pt/C. The performance and decay rate of Pt/WC/C were also evaluated in a fuel cell.

1. Introduction

One of the main factors limiting the lifetime of proton exchange membrane fuel cells (PEMFCs) is the degradation of the electrocatalyst layer, in particular, corrosion of the carbon support [1–5]. The corrosion rate of carbon black at potentials lower than 0.9 V is reasonably slow at the typical operating temperatures (60–90 °C) of the PEMFCs. However, long-term operations can cause a decrease in carbon content in the catalyst layers [3]. In particular, during extended operation with start–stop cycling and fuel starvation, the cathode can experience high potentials up to 1.5 V [6,7]. Under these conditions, severe carbon corrosion occurs, causing catalyst particle agglomeration, and increasing the ohmic resistance and the gas diffusion resistance due to collapse of the porous structure. More stable support materials are strongly needed to improve the stability and durability of the catalyst layers [3].

Metal carbides, especially tungsten monocarbide (WC), have been proposed as catalyst support for fuel cells due to their high stability, low electrical resistivity, and strong interaction with the metal catalysts [8–16]. Chhina et al. [12] compared the stability of Pt supported on tungsten carbide to that supported on Vulcan XC-72 and found that the former could retain the surface area and activity better during the corrosion testing in acid. The high stability of tungsten carbides in the electrochemical testing was assigned to a core–shell type structure that was formed when the surface of tungsten carbides were oxidized to WO*x*, forming a passive shell encapsulating the carbide core. It is important, however, to note that the stability of tungsten carbides also depends on the structure, phase, and shape. For instance, it has been reported that WC is more stable than W_2C in the acidic medium [10,17].

In addition to the high stability, tungsten carbides are also expected to enhance the catalytic activity of the Pt nanoparticle due to the strong metal–support interaction (SMSI) [18]. Shen's group reported that the oxygen reduction reaction (ORR) activities of Pt and Pd based catalysts were enhanced significantly on the tungsten carbides modified carbon supports [19–22]. The possible reasons for the observed activity enhancement include more uniform catalyst distribution on the modified carbon and the synergistic interaction between metal particles and tungsten carbides. Such interaction may cause some change in electronic environment of Pt leading to low oxide formation on the surface of Pt, which is believed to be one of the causes for Pt dissolution [1].

The synthesis of high surface area WC as the support for Pt catalyst is a great challenge. One alternative way to take advantage of the high stability and SMSI of WC is to coat the high surface area carbon black with a relatively uniform nano-structured WC coating (film or small nanoparticles). Several previous studies reported the modification of carbon support with large carbides powder mixed with WC and W_2C phases [8,12,23]. In the present work, we focus

* Corresponding authors. Tel.: +1 860 727 7251; fax: +1 860 660 7384.
E-mail addresses: Minhua.shao@utcpower.com (M. Shao), jgchen@udel.edu (J.G. Chen).
[1] Current address: Center of Excellence in Nanotechnology (CENT) & Department of Chemistry, KFUPM, Dhahran 31261, Saudi Arabia.

0378-7753/$ – see front matter © 2011 Elsevier B.V. All rights reserved.
doi:10.1016/j.jpowsour.2011.04.026

on the synthesis of phase pure WC nanoparticles on high surface area carbon black, the effect of the WC on the corrosion resistance of carbon black and ORR activity and stability of Pt, and the stability of WC itself during potential cycling. The activity and durability of Pt catalysts supported on phase pure WC modified carbon were also tested in the fuel cell for the first time.

2. Experimental

2.1. Carbides synthesis

The carbides were coated on the Ketjen Black EC300J (Akzo Nobel) by a temperature programmed reaction (TPR) method. Ammonium metatungstate hydrate (Aldrich) was mixed with deionized water and stirred until complete dissolution. The solution was added dropwise to Ketjen Black powder in a beaker while mixing with a metal stirring rod. This mixture was dried in an oven at 70 °C for 24 h and then placed in a quartz tube furnace under 1.3% hydrogen gas and 4.0% methane gas with a flow rate of GHSV: 1000 h^{-1}. It was heated to 450 °C over 2 h, followed by an increase to 975 °C over 8 h. It was held to react with hydrogen and methane at 975 °C for 1 h, then allowed to cool down. Finally, the sample was passivated with a mixture of 1% O_2 and 99% N_2 for 1 h to mildly oxidize the surface defects before exposing to air.

2.2. Deposition of Pt nanoparticles on WC-modified carbon black

Two grams of WC coated Ketjen Black powder (WC/KB) were dispersed in 200 ml of MilliQ UV-plus water (Millipore) and magnetically stirred for 15 min. The suspension was ultrasonically blended at 200 W for 5 min and then magnetically stirred for 5 min. This step was repeated three times. 3.2 g of hexacholoroplatinic acid (Alfa Aesar) was dissolved in 20 ml of water and added dropwise and mixed in an ultrasonic bath for 30 min. Carbon monoxide (20% balanced with N_2) was then flowed at 200 ml min^{-1} for 1 h while the mixture was heated to 90 °C. The platinum salt was reduced using 5 ml of 37% formaldehyde (Aldrich) added dropwise over a period of 10 min with CO flowing. After being filtered, the catalyst was washed with water thoroughly and allowed to dry in a vacuum oven at 80 °C. The Pt loading was measured by the inductively coupled plasma (ICP) to be 40 wt.%. The similar procedure was applied to synthesize supported Pt on bare Ketjen Black powder for comparison.

2.3. Electrochemical testing

The active material was mixed with PTFE emulsion as a binder (6 wt.%). The mixture was then fiberolized until a paste was obtained by thoroughly mixing with isopropyl alcohol (IPA). The paste was pressed into an approximately 500 μm thick and 1.2 cm diameter disc using a pellet press. The pellet electrode was washed with water and IPA to remove traces of impurities and to enhance the material utilization during the corrosion process. To measure the initial weight, the pellet electrode was dried under vacuum and nitrogen at 85–90 °C for at least 5 h to remove all traces of alcohol and water. Prior to the corrosion test, the pellet electrode was soaked in the working electrolyte (0.5 M H_2SO_4) overnight to assure that electrolyte penetrates into the pores. The pellet was then attached to a gold disc substrate which served as a sample holder and current collector. For corrosion test, the pellet was placed in a three-electrode electrochemical jacketed cell with a reversible hydrogen electrode (RHE) as a reference electrode and Pt gauze as a counter electrode, separated from the working electrode compartment by a fritted glass tube. Electrochemical measurements were carried out in a nitrogen saturated 0.5 M H_2SO_4 solution (GFS) at 1.4 V and 80 °C for a period of 5 h. Prior to the potential hold, the electrode was cycled for several cycles between 0 and 1.2 V to assure that the active material was fully wet and to take an initial CV for comparison. After the corrosion test, the pellet electrode was subjected to a few cycles before taking the final CV. Then, the pellet was soaked in pure DI-water overnight to remove any trace of electrolyte prior to the drying process. Before measuring the weight of the tested electrode, the pellet was dried under vacuum and nitrogen at 85–90 °C overnight to remove any trace of water. Corrosion rates were estimated from both the weight change and charge passing through the electrode. It is important to note that the rate based on charge was always higher than that based on weight change since the corrosion process involves the formation of metal oxides, which cause weight gain. It was also noticed that KB carbon did show weigh gain instead of weight loss.

The electrochemical behavior of Pt deposited on WC-modified carbon was characterized by cyclic voltammetry. Approximately 15 mg of the powder was dispersed in a solvent consisting of 12 ml of water, 3 ml of isopropanol, and 60 μl of 5% Nafion (Aldrich) by ultrasonication for 10 min. 10 μl of the suspension was deposited on the pre-cleaned glassy carbon substrate (Pine Instruments) and allowed to dry. A reversible hydrogen electrode and Pt mesh were used as a reference and counter electrode, respectively. The catalyst was cycled from 0.02 to 1.2 V until a stable CV was obtained (generally 10 cycles). The ORR activity was evaluated in an oxygen saturated 0.1 M $HClO_4$ solution using the rotating disk electrode (RDE) technique at a rotation speed of 1600 rpm. The durability of the catalysts was also investigated under potential cycling. The potential of the electrode repeatedly switched from 0.65 to 1.2 V every 5 s for up to 20,000 cycles using square-wave signal. The ORR activity and the electrochemically active area (ECA) were measured in a fresh 0.1 M $HClO_4$ solution every 5000 cycles.

2.4. Fuel cell testing

The catalyst powders were deposited onto a decal with a Mayer-rod coater. The electrode was transferred onto a bare membrane (25 μm) by hot pressing at 130 °C and 26.7 kN for 10 min. A standard anode of 0.3 mg Pt cm^{-2} and the same membrane were used for all builds.

The Pt loading of the electrode was determined by measuring the mass of the decal before and after hot pressing. The Pt loadings were 0.36 and 0.31 mg cm^{-2} for Pt/KB and Pt/WC/KB, respectively. The weight percent of Nafion® in the electrode was determined by measuring the weight loss as the electrode was ramped from room temperature to 700 °C in a nitrogen environment using a Thermal Gravimetric Analyzer (TGA) with the assumption that only water and Nafion were removed. The Nafion content was found to be ~38% for both Pt/KB and Pt/WC/KB samples. The weight percent of Pt in the catalyst was determined using ICP.

Each cell was conditioned by cycling until peak performance was achieved (about 60 h). A cycle consisted of stepping the load from 100 mA cm^{-2} to a maximum current density and back to 100 mA cm^{-2} in 100 mA cm^{-2} increments. The maximum current density was the maximum current at which a voltage greater than 0.35 V could be sustained.

Following conditioning, the performance of the MEA was assessed. The fuel, air and oxygen utilization was 25%, 25% and 5%, respectively. The cell temperature was 75 °C. An orifice downstream was used to maintain a backpressure of 100 kPa. The load was ramped from OCV to 0.25 V at intervals of 10, 50, 100, 200, 300 mA cm^{-2}, etc.

Degradation of the cell performance was tested with two different protocols, either potential hold at 1.2 V or potential cycling between 0.6 and 1.0 V. Both protocols were controlled by a potentiostat in a hydrogen/nitrogen environment. The potential cycling consisted of a square wave with a 5 s hold at 0.6 V followed by a

5 s hold at 1.0 V. The potentials and hold times were selected for a balance of Pt dissolution and carbon corrosion. All potentials are given with respect to a reversible hydrogen electrode (RHE).

2.5. Characterization

XPS measurements were made using a Phi 5600 XPS system with an Al anode X-ray source and a multi-channel hemispherical analyzer. An anode potential of 12 kV and an emission current of 20 mA were used for measurements. The XPS system was calibrated using indium foil as a reference. Peaks were compared to known literature values for specific elements and compounds [24].

TEM images were taken using an FEI Tecnai F20 transmission electron microscopy (TEM) with a Field Emission Source at 200 keV. A dispersion of the catalyst in ethanol was placed on a 3 mm Cu grid coated with a carbon film and allowed to dry.

Powder X-ray diffraction patterns (XRD) were taken by a commercial diffractometer (Bruker AXS D8 Discover) using Cu Ka radiation ($\lambda = 1.54056$ Å). Samples for analyses were obtained by filtering the WC-modified Ketjen Black suspension on filter paper and transferring it to a carbon paper (7 cm × 7 cm) by pressing. After drying, the carbon paper was cut into small pieces with an area of 1 cm^2 to undergo potential cycling. Diffraction patterns of potential cycled samples were collected from 20 to 90° with a step size of 0.02°.

X-ray Absorption Near Edge Structure (XANES) measurements of Pt were carried out at the National Synchrotron Light Source (NSLS), Brookhaven National Laboratory (BNL) using Beam Line X18B. The XAS data were processed using the IFEFFIT analysis package. The samples for XANES measurements were prepared by coating the catalysts powder on a carbon paper with a Pt loading of 1 mg cm^{-2}.

3. Results and discussion

3.1. Synthesis and characterization of WC-modified carbon black

In general, carbides can be formed by sacrificial reaction of carbon with metal oxides. This generally leads to bulk carbides with low surface area [12]. The temperature programmed reaction (TPR) method has gained more attention since it leads to surface modified carbon (surface metallization) without dramatic loss in carbon surface area. Using CH_4 and H_2 as the gas phase reagents, it is feasible to scale up the synthesis of carbide-modified carbon in the range of grams to kilograms depending on the size of the reactor. In the current study high surface area carbon, i.e., Ketjen Black, was selected as the substrate to modify with WC using TPR to achieve a high surface area and stable support.

Fig. 1 shows the XRD patterns of tungsten carbide modified Ketjen Black with a metal W loading of 20 wt.%. A mixture of WC and W_2C phases were formed when the WO_3/KB precursors were kept at 850 °C for 1 h in the presence of CH_4 and H_2 with a ratio of 1:4. This sample is denoted as WxC/KB. By increasing the reaction temperature to 950 °C and keeping the same CH_4/H_2 ratio, only the diffraction patterns from WC phase were observed, suggesting the absence of W_2C phase in the product. This sample is denoted as WC/KB. This is the first time that phase pure WC is synthesized on high surface area Ketjen Black carbon by the TPR method to the best of the authors' knowledge. WC is more stable than W_2C in acid media. Zellner and Chen demonstrated that the oxidation and dissolution of WC did not occur at potentials below 0.6 V (NHE) [25], while the oxidation of W_2C started at as low as 0.2 V (NHE) [17]. Hence, the phase pure WC is more desirable for fuel cell applications.

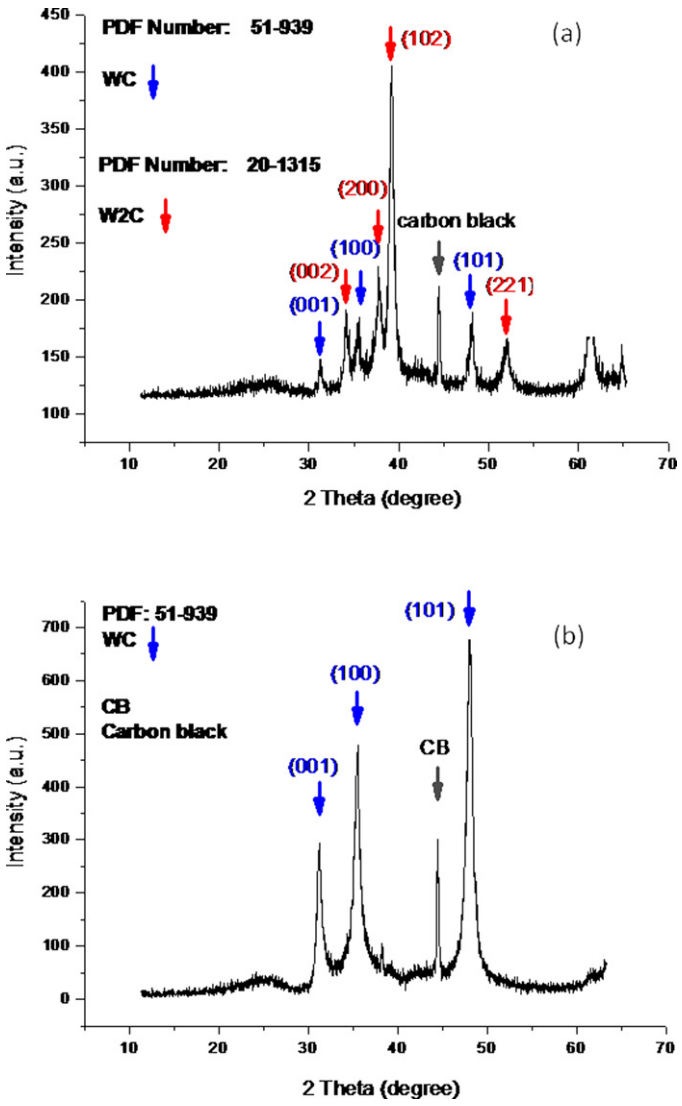

Fig. 1. XRD patterns of WxC (a) and WC (b) modified Ketjen Black.

A typical TEM image of WC modified Ketjen Black is shown in Fig. 2a. The Ketjen Black particles were not uniformly covered by individual nanocrystaline WC, with most of the particles (~70%) in the range of 2–30 nm. A few particles larger than 100 nm were also observed. We believe that the coverage can be improved further by optimizing the process, especially during the impregnation of the salt into carbon. Chhina et al. [8] synthesized phase pure WC with agglomerates ranging from 5 to 9 μm by sacrificing most of the carbon black powders (Vulcan XC-72R) at 1100 °C, which were the source of the carbon atoms. The BET area of Vulcan XC-72R decreased from 250 $m^2\ g^{-1}$ to 0.6 $m^2\ g^{-1}$ in Chhina's samples. With the TPR method, the high BET area of carbon black can be maintained because it only sacrifices the carbon atoms at the surface. The BET area of Ketjen Black after 20% of WC deposition was reduced from 800 $m^2\ g^{-1}$ to 435 $m^2\ g^{-1}$, which is still highly sufficient as a fuel cell catalyst support. Fig. 2b and c shows TEM images for the platinized KB and WC/KB, respectively. The average Pt particle size for Pt/WC/KB (3.5 nm) is slightly larger than that of Pt/KB (3 nm). This indicates that the surface area of WC/KB does not significantly affect the Pt particle size. The EDS spectrum of Pt/WC/KB (not shown) reveals a weight ratio of W:Pt = 1:3.5, which is in good agreement with the ratio (1:3.4) based on ICP measurements.

In addition to XRD and TEM analyses, changes in the XPS binding energy clearly show the formation of WC on the carbon surface.

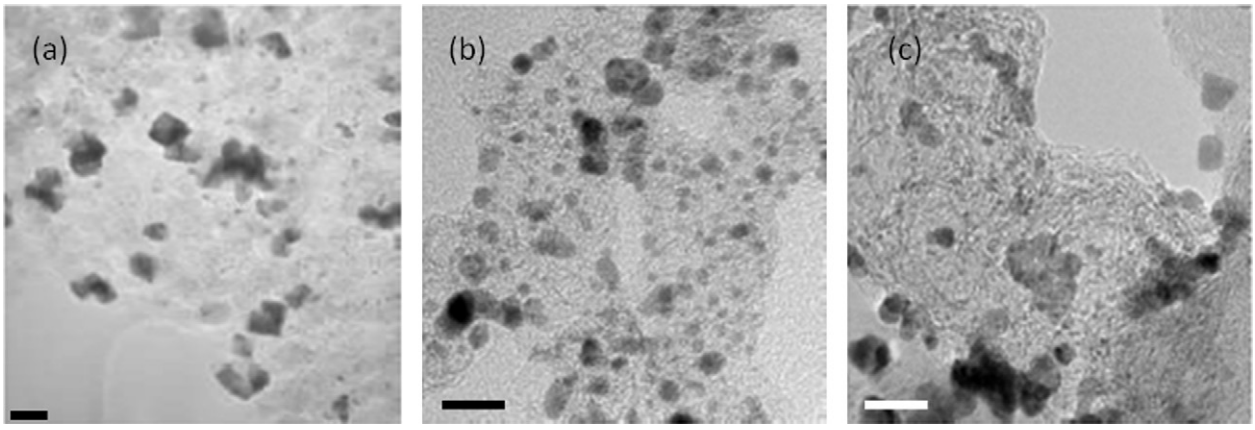

Fig. 2. TEM images for WC modified KB (a), Pt/KB (b) and Pt/WC/KB (c). The scale bar in (a), (b) and (c) is 50, 10 and 10 nm, respectively.

Fig. 3 shows that the two W4f peaks are characteristic of W in the carbide form [25], confirming the presence of WC on the surface of the sample. The C1s peak is dominated by that of graphitized carbon at 284.5 eV, because the signal from the KB substrate outweighs the signal for WC. The detection of the relatively weak feature in the O1s region is likely from the adsorption of oxygen-containing molecules upon exposing WC to air.

3.2. Corrosion test of carbides

The corrosion behavior of tungsten carbides modified Ketjen Black was examined by measuring the current density profile at 1.4 V. Fig. 4 shows the changes in current densities (normalized to the weight of the carbon, noted as mA mg^{-1} C) of W*x*C/KB, WC/KB, and KB samples. The electrodes were subjected to a potential of 1.4 V in 0.5 M H_2SO_4 for 5 h at 80 °C. As expected, the current densities of all three samples decreased quickly during the first 1 h of the potential hold and reached a similar current density after the 5-h testing. In the first 20 min, the WC/KB sample showed a better corrosion resistance than any other sample, with the similar trend being observed even at the end of experiment. The decrease in the current density may be due to passivation of the surface as a result of oxide formation. In other words, the surface oxides increase the interfacial contact resistance leading to low passing current. Based on these results, the rate of the corrosion current density during the first 1-h of testing follows the order of KB > W*x*C/KB > WC/KB, sug-

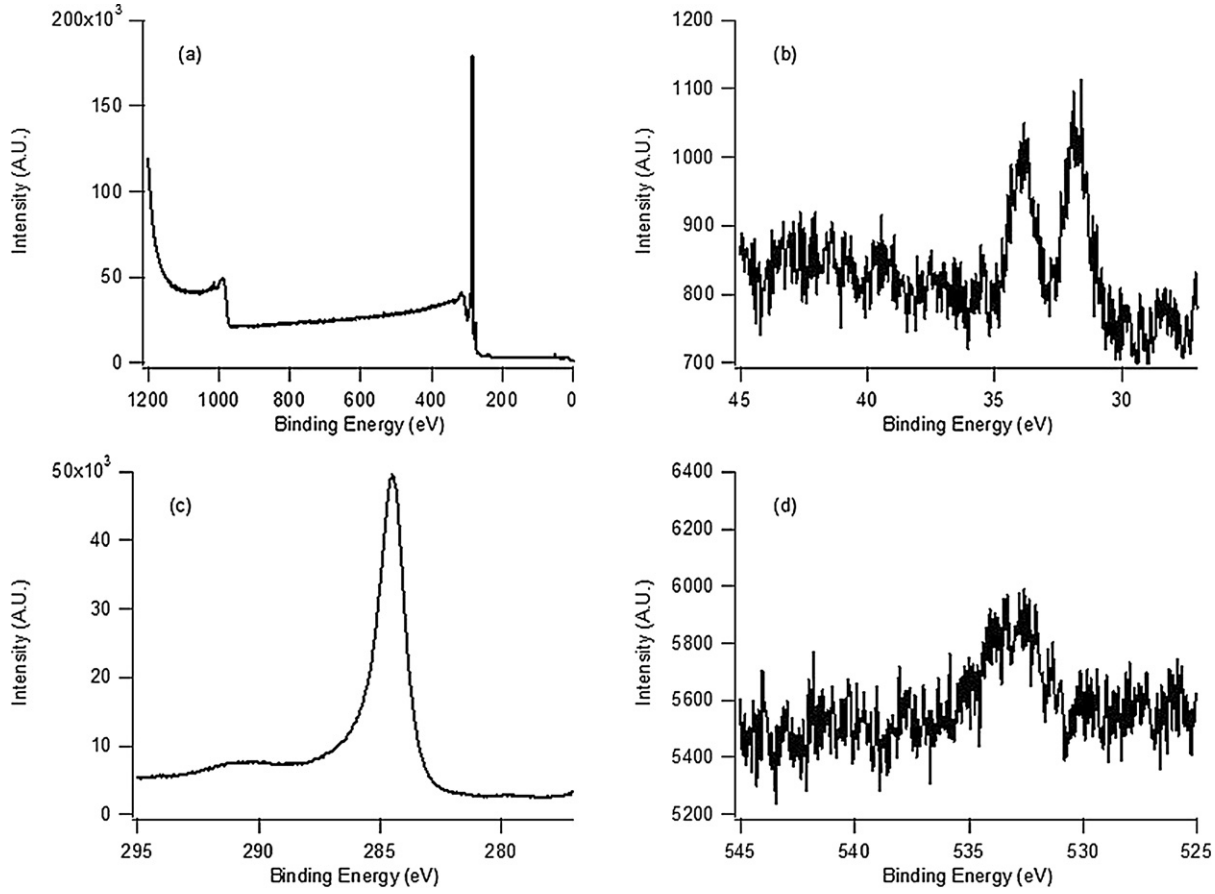

Fig. 3. WC modified KB XPS wide scan spectra (a), W4f peak (b), C1s peak (c), and O1s peak (d).

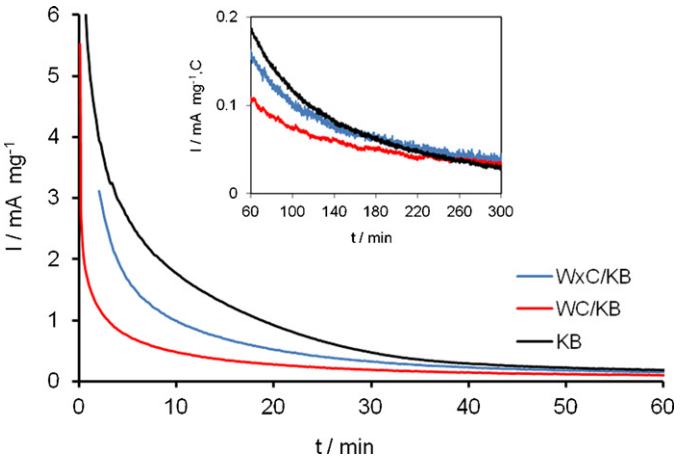

Fig. 4. Comparison of current normalized to the weight of carbon for different catalyst supports. The supports were kept at 1.4 V in 0.5 M H_2SO_4 solution at 80 °C.

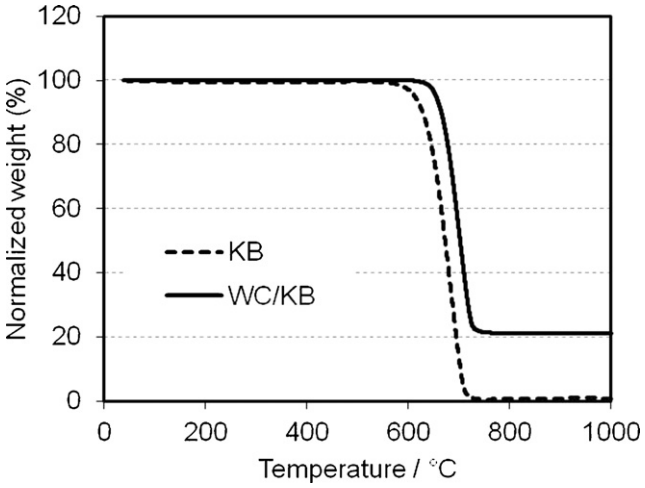

Fig. 5. Normalized weight loss vs. temperature profiles for bare and WC treated KB. The temperature was ramped at 10 °C min^{-1} and the oxidation was performed in air.

gesting that the passivation of WC modified KB is much faster than that of bare KB due to the partial coverage of the carbon surface by WC. These results also confirm that the phase pure WC is more stable than W*x*C, in good agreement with the literature [17,25].

Table 1 summarizes the weight change of the samples and the corrosion rates estimated from the electrode charge. All samples show weight gains, indicating the formation of oxygen-containing species on the surfaces. For carbides modified samples, the weight gains are larger than the bare KB, which makes sense since the density of WO*x* is much higher than that of functional groups, such as C–O, COO–, and =C=O. Hence, the corrosion rate based on the specific charge normalized to the weight of the carbon in the samples follows the order of KB > W*x*C/KB > WC/KB. This trend reveals that depositing WC on the surface of carbon is beneficial from a corrosion point of view. Moreover, it is worthwhile to note that the formation of the WO*x* layer may increase the interaction between metal catalyst and the support, potentially leading to synergistic effects on activity and stability.

When an electrode is exposed to high voltage, such as 1.4 V in the current experiments, the electrochemical properties are expected to change dramatically. In a fuel cell environment there are two undesirable processes involving the support: (i) the catalyst detachment from the support at high potentials due to the lack of interaction between the metal particles and the carbon [26] and (ii) the electrochemical corrosion of the support causes catalyst particle agglomeration due to loss of surface area, an increase in resistance of gas diffusion due to the collapse of porous structure and oxide formation, and an increase in ohmic loss due to a presence of less conductive carbon surface [3]. The latter is a more common phenomenon in fuel cells as clearly demonstrated by Ioroi et al. [27] and Chhina et al. [28]. Therefore, a suitable support is needed to maintain fuel cell performance by minimizing the weight loss and surface oxide formation. The corrosion testing results demonstrate that the charge passed for KB due to carbon corrosion can be reduced by modification of the surface with a WC layer. Ideally, one can optimize the WC/KB system in order to have a better WC coverage on the surface. We believe that this can be achieved after further investigation on the impregnation method and loading.

Table 1
Corrosion data for tungsten carbides modified KB*.

Sample	Weight change	Specific charge (C mg^{-1}, carbon)	Rate based on charge (μg h^{-1} mg^{-1}, carbon)
KB	4–5% gain	4.6	28.8
20% WC + W_2C/KB	6.0% gain	2.87	17.53
20% WC/KB	7.0% gain	1.95	12.12

* The potential of the samples were held at 1.4 V in 0.5 M H_2SO_4 at 80 °C for 5 h.

3.3. TGA analysis of WC effect on carbon oxidation

In order to gain more information on the WC effect on the corrosion resistance of KB, the gas phase oxidation of KB and WC/KB was studied by TGA. The TGA method is a useful accelerated degradation testing method for assessing the dimensional stability and oxidation/corrosion resistance of carbon support [29,30], since there are parallels between the relative thermal stability in an oxygen-containing atmosphere and the relative support stability in an operating fuel cell. The profile of normalized weight vs. temperature is shown in Fig. 5. For the bare KB sample, there is nothing left after the TGA measurement due to the complete gasification of the sample. However, about 20% weight remains for the WC/KB sample indicating the existence of the tungsten oxide species (WO*x*). The onset temperature for the weight loss due to gasification of carbon was different for these two samples. The onset temperature shifted to a higher temperature by ~50 °C with a WC coating. This reveals the degradation resistance of WC at high temperature and in the presence of air. The oxidation of carbon powder initiates at the surface defects and graphitic edge plane sites. The delayed oxidation of carbon implies that those sites may be covered by WC. Once the oxidation starts, the gasification of the carbon progressively increases the pore/defect size allowing deeper penetration of oxygen into the powder interior. Thus, after the oxidation initiates, the WC coating does not prevent further corrosion of the carbon. This argument agrees with Fig. 5, which shows a similar corrosion rate of carbon for the bare and WC coated KB after passing the initial stage of oxidation. We believe that the stability of carbon can be further improved by increasing the dispersion of WC on KB. The higher the WC coverage is, the better stability can be achieved.

3.4. Durability test of WC/KB with potential cycling

During extended operation with start–stop cycling, the cathode can experience more severe carbon corrosion than potential holding [7]. Previous studies demonstrated that WC film was not stable at high potential and underwent oxidation to form WO*x* and dissolved in the acid solutions. In order to gain more durability

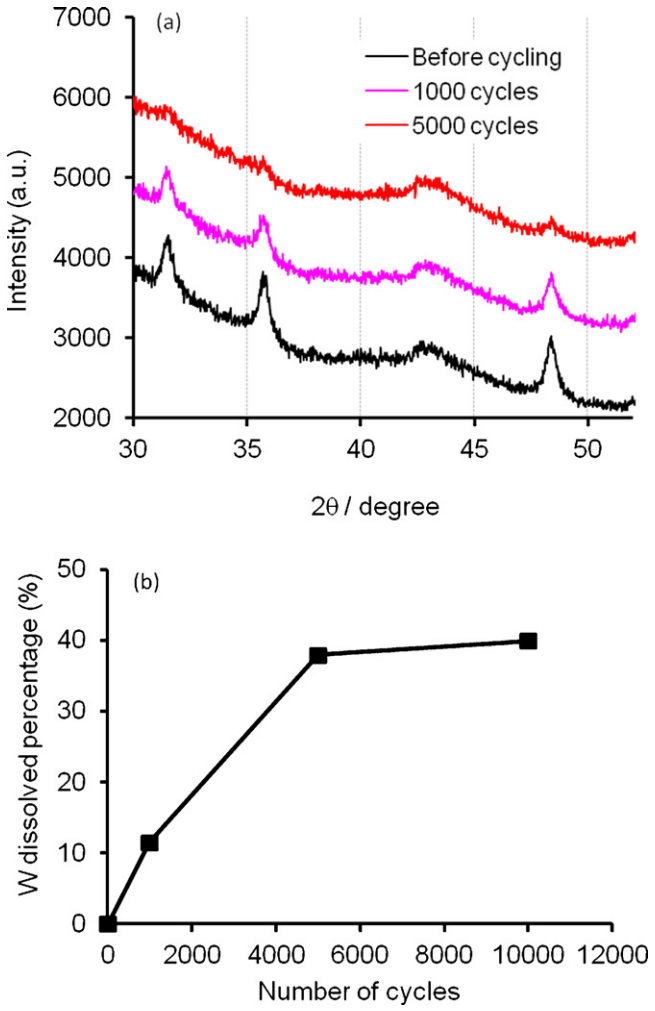

Fig. 6. Comparison of XRD patterns of WC/KB before and after potential cycling (a) and dissolved tungsten as a function of number of cycles measured by ICP (b). Potential cycling protocol: 0.65 V (5 s)–1.2 V (5 s) in a 0.1 M $HClO_4$ solution saturated with O_2.

information on the WC/KB system, potential cycling experiments were performed. Fig. 6 shows the XRD patterns of WC/KB coated on carbon paper during potential cycling in an oxygen-saturated 0.1 M $HClO_4$ solution. The potential was kept at 0.65 V for 5 s and switched to 1.2 V and kept at this potential for another 5 s. After 1000 cycles, the diffraction peaks ascribed to WC were weakened compared to those without cycling, suggesting the loss of WC on the electrode. Additional potential cycling causes further loss of WC. After 5000 cycles, only traces of WC were detectable, indicating almost complete loss of WC phase on the surface. The amount of dissolved W in the acid solution was monitored by ICP. The results are shown in Fig. 6b. Even though the XRD data suggest a complete loss of WC, the dissolved W is only about 40% of the total W deposited on KB after 5000 potential cycles, in agreement with the EDS data, which shows 50% of W remains in the sample. Based on the above information, it is possible that one part of the WC particles dissolved into solution and rest of them were oxidized to form WO*x* during potential cycling. However, it should be noted that dissolution of WC and its structure change may also depend on the type of acid medium because the perchloric acid releases Cl^- during cycling and may cause the dissolution of WO*x* formed on the surface. Perhaps this is the reason that ICP has shown that almost 40% of W was dissolved. In fact, these conditions do not represent a fuel cell environment. It is very important to conduct studies in different acids.

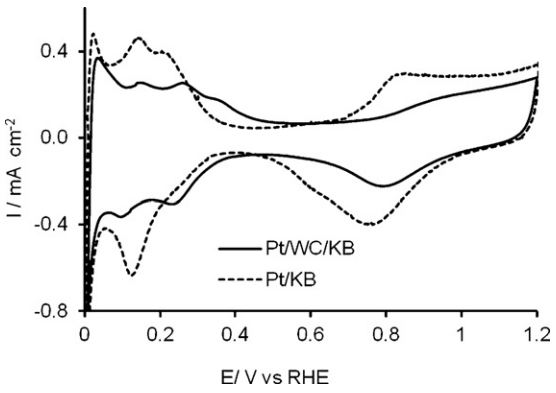

Fig. 7. Cyclic voltammograms of Pt/WC/KB in a 0.1 M $HClO_4$ solution saturated with N_2 compared with that of Pt/KB.

Hence, further investigation will be conducted in the future in this regard.

3.5. Electrochemical behavior of Pt on WC/KB

Fig. 7 shows the cyclic voltammetry curves of Pt supported on bare and WC modified KB in a nitrogen-saturated 0.1 M $HClO_4$ solution. The features in the hydrogen adsorption/desorption area are quite different for these two samples. The peaks associated with H_{UPD} on the {1 1 0} and {1 0 0} facets are more pronounced for Pt/WC/KB than Pt/KB due to the larger particle size of the former. An extra current peak at 0.35 V in the positive scan was observed for Pt/WC/KB resulting from the hydrogen spill-over from Pt or the formation of tungsten bronzes [12,31]. The existence of this peak indicates that WC particles remain on the carbon black after Pt deposition and contact with some Pt nanoparticles.

The WC is partially oxidized in air and covered by a layer of WO*x* forming a core–shell structure. The surface oxide plays a great role not only in corrosion protection of WC, but also may provide a strong interaction with Pt particles resulting in an enhanced oxygen reduction activity (ORR) and stability. The oxygen reduction activity of Pt/WC/KB was tested by the RDE technique and compared to that of Pt/KB. In this work, we found that similar Pt mass activities were obtained for Pt/WC/KB (0.15 A mg^{-1}, Pt) and Pt/KB (0.14 A mg^{-1}, Pt).

To investigate the impact of support on catalyst durability, platinized samples were subjected to potential cycling between 0.65 and 1.2 V for 5 s each in an oxygen-saturated 0.1 M $HClO_4$ solution at the room temperature. Fig. 8a shows the CV curves of Pt/WC/KB after 5000 and 10,000 potential cycles. Compared to the pristine sample, the change in the hydrogen adsorption/desorption region decreases significantly and the current density peaks from {1 0 0} and {1 1 0} remain, while the peak at 0.35 V disappears after 5000 cycles. The absence of the current density peak associated to the hydrogen spill-over from Pt to WC implies that the amount of WC decreases dramatically, in good agreement with the XRD shown in Fig. 6. The charge associated to Pt oxide reduction is much smaller than that of hydrogen adsorption/desorption indicating that most of the current reduction in the hydrogen region is caused by the loss of WC, i.e., the absence of H spill-over. Similar results have been reported on Pt particles supported on bulk WC powders [12]. The ORR activities of the samples were measured after every 5000 cycles and shown in Fig. 8b. Most of the activity decay for both Pt/KB and Pt/WC/KB occurs in the first 5000 cycles due to severe Pt particle size growth and dissolution (Fig. 8c). The activity decay rate of Pt/WC/KB is lower than that of Pt/KB due to slightly larger particle size of the former and/or strong interaction between Pt and WC/WO*x*.

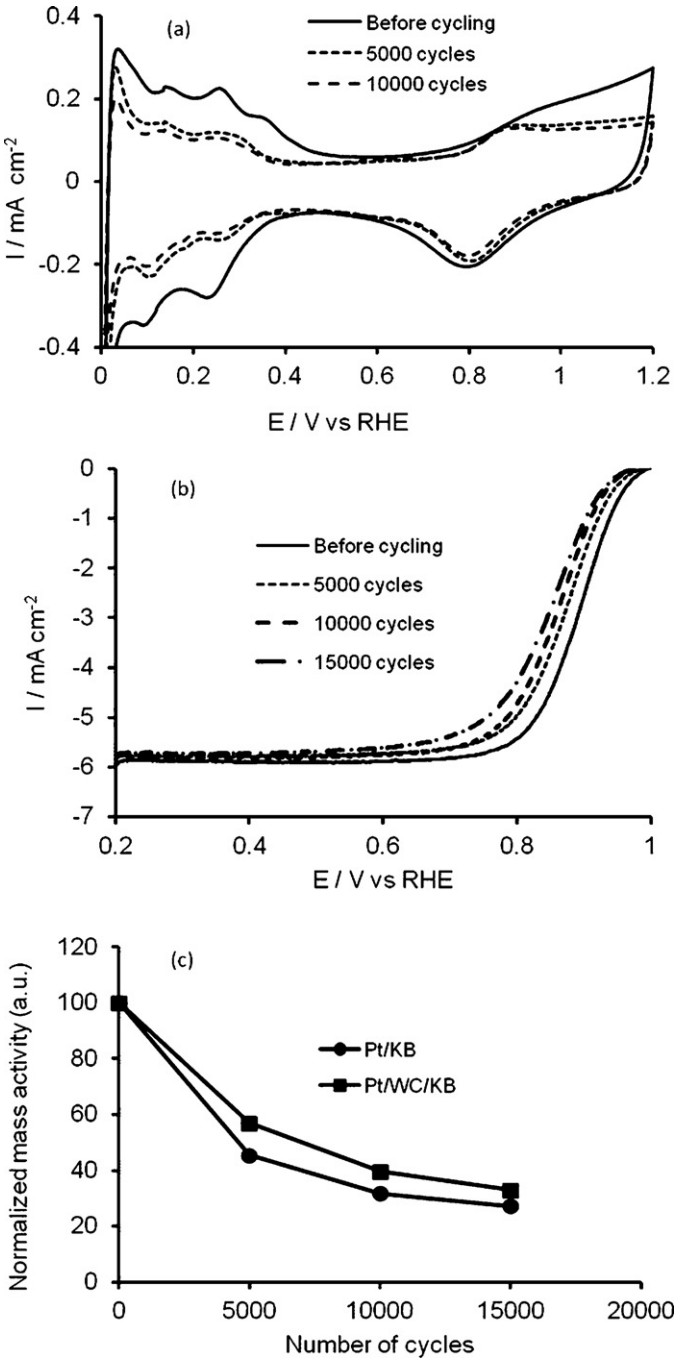

Fig. 8. Cyclic voltammograms of Pt/WC/KB before and after potential cycling (a), ORR curves (b), and ORR activity changes during potential cycling compared to Pt/KB (c). The potential scanning rates for (a) and (b) are 50 and 10 mV s^{-1} in a nitrogen- and oxygen-saturated 0.1 M $HClO_4$ solution, respectively. The rotation speed in (b) is 1600 rpm.

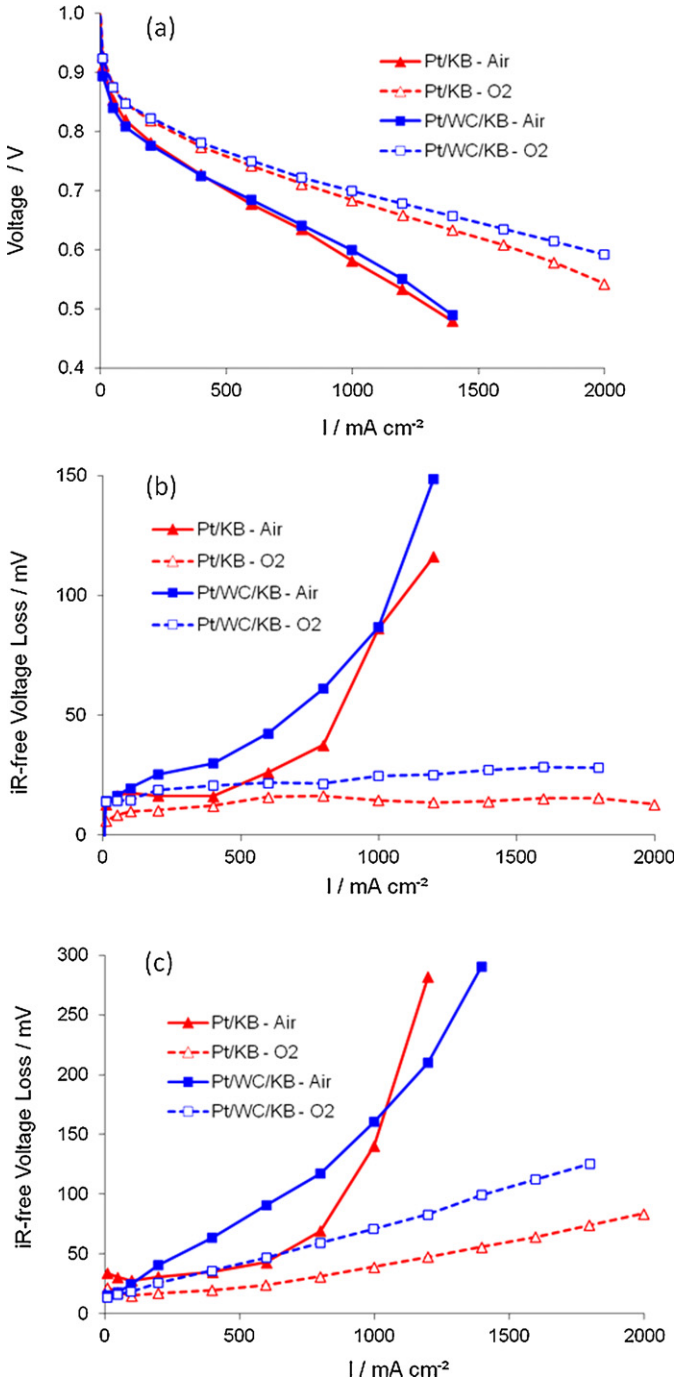

Fig. 9. (a) Performance curves on H_2/air and H_2/O_2 for Pt baseline catalyst (red triangles) and Pt/WC/KB (blue squares). Dashed lines represent H_2/O_2 data, solid lines represent H_2/air data. (b) Potential cycling performance loss (difference between voltage before potential cycling and voltage after potential cycling) on H_2/air and H_2/O_2 for Pt baseline catalyst (red triangles) and Pt/WC/KB (blue squares). Dashed lines represent H_2/O_2 data, solid lines represent H_2/air data. (c) Potential hold performance loss (difference between voltage before potential hold and voltage after potential hold) on H_2/air and H_2/O_2 for Pt baseline catalyst (red triangles) and Pt/WC/KB (blue squares). Dashed lines represent H_2/O_2 data, solid lines represent H_2/air data. (For interpretation of the references to color in this figure legend, the reader is referred to the web version of this article.)

3.6. Fuel cell test

The Pt/WC/KB catalyst was tested for performance and durability in a 25 cm^2 fuel cell and compared against the performance and durability of a Pt/KB catalyst. To the best of the authors' knowledge, this is the first report of fuel cell testing on WC (single phase) based support. The performance in air and oxygen is shown in Fig. 9a for both catalysts under given conditions. The Pt/WC/KB catalyst showed a similar performance to the Pt catalyst in both air and oxygen, in agreement with the RDE measurements. In the high current density region (mass transport region), the performance of Pt/WC/KB was slightly better than that of Pt/KB. Such behavior could be associated with a low peroxide formation rate as a result of the effect from WO_x layer [32,33], and a better mass transport in the Pt/WC/KB electrode.

The durability of the catalyst was tested by both potential cycling between 0.6 and 1.0 V, and potential hold at 1.2 V. The performance was assessed before and after the durability testing and the results are given as the difference in the iR-free voltage loss at the same current density. The voltage loss due to potential cycling is given in Fig. 9b. The voltage loss in oxygen remains constant with current density, which would indicate an activity loss. The Pt on carbide had about 25 mV activity loss while the Pt on carbon had about 15 mV loss in oxygen. The performance loss in air includes the activity loss as well as mass transport losses. The performance loss increases exponentially at high current density, suggesting decreased mass transport as the limiting current decreases. Increased carbon corrosion generally increases the water retention in the catalyst layer resulting in lower mass transport. The change in hydrophilicity and pore structure of the electrode was not characterized to confirm this hypothesis.

The durability was also assessed after a potential hold for 24 h at 1.2 V. The voltage loss due to the potential hold is given in Fig. 9c. The voltage loss in oxygen shows an activity loss at low current densities as well as a linear increase for both the Pt/WC/KB and the Pt/KB catalysts. A linear increase would indicate an increase in electrode resistance which may be due to increase in contact resistance between catalyst and support particles. The voltage loss in air included the activity and iR loss as well as mass transport loss that increased at high current densities. The overall performance loss was higher for the Pt/WC/KB catalyst than the Pt/KB catalyst, except above 1000 mA cm^{-2} where the Pt/KB had a sharper increase in voltage loss. The reasons for the larger performance loss observed in the fuel cell testing for Pt/WC/KB were not fully understood. It may be related to the formation of WO*x*, which is more hydrophilic than carbon, resulting in a larger gas mass transport loss.

3.7. Interaction between Pt and WC

In addition to electrochemical evaluation, XPS and XANES were applied to investigate the catalyst–support interaction. Fig. 10a shows the XPS spectra for Pt_{4f} of different samples. The Pt $4f_{7/2}$ and Pt $4f_{5/2}$ bands were observed at 71.6 eV and 74.9 eV for as synthesized Pt/KB sample. It is possible that some of the Pt surface atoms were not fully reduced by formaldehyde during the catalyst synthesis. Thus, the as-synthesized catalysts were further reduced in 5% H_2 balanced with Ar at 350 °C for 30 min. The Pt $4f_{7/2}$ and Pt $4f_{5/2}$ bands for the samples reduced by H_2 were found to be ~0.15 eV lower than the as-synthesized sample. The binding energies of the Pt_{4f} for Pt/WC/KB are identical to those for Pt/KB indicating no strong effect on the oxidation state of Pt from the interaction with WC. To gain more structural and electronic information on the WC modified sample, XANES measurements have been carried out. Fig. 10b compares the normalized XANES spectra of Pt L_2 edge for Pt foil and supported Pt catalysts. The Pt L_3 edge has a much stronger intensity than the L_2 edge and is more desirable for XANES analysis. However, the Pt L_3 spectrum is significantly interfered by the W L_3 edge. The as synthesized Pt/KB sample showed large white line intensity due to the incomplete reduction of the Pt atoms, in agreement with the XPS data. The shape and intensity of the Pt L_2 edges are similar for Pt/KB and Pt/WC/KB after H_2 reduction indicating no significant electron transfer between WC and Pt. The results of density functional theory (DFT) calculations revealed a strong interaction between WC and Pt clusters and consequently a significant change in the electronic property of Pt [18]. The low coverage of WC particles on carbon surface in our samples may be one of the main reasons for the observation of a weak metal–support interaction since only a small part of Pt particles are contacting with WC.

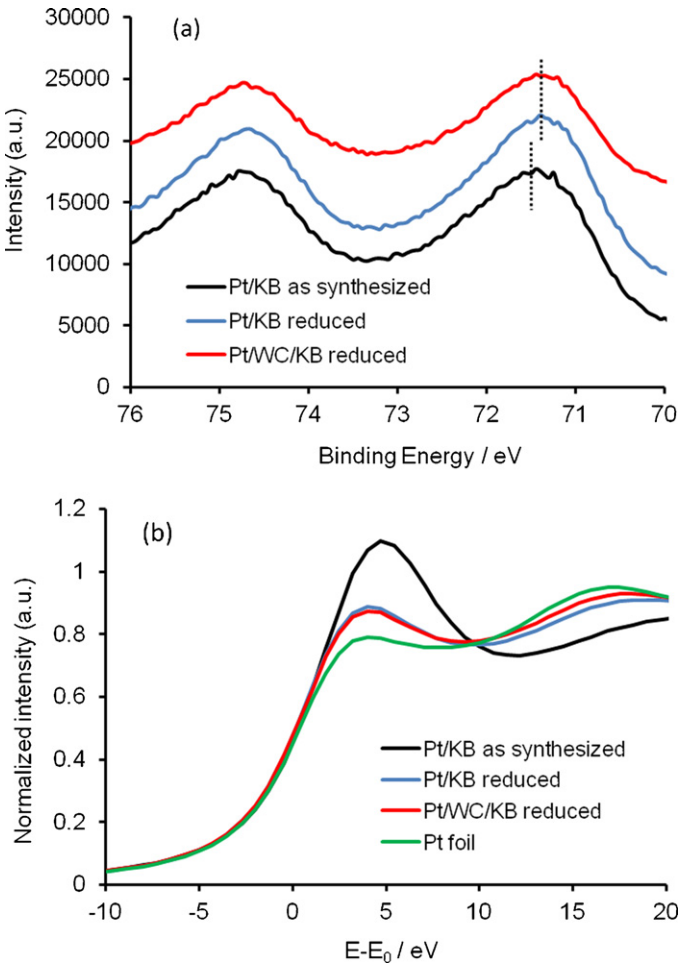

Fig. 10. XPS spectra of Pt 4f (a) and XANES for Pt L3 edge (b) for Pt catalysts supported on bare and WC modified Ketjen Black. The spectra for Pt/KB before and after reduction in H_2 atmosphere at 350 °C were also compared.

4. Conclusions

Phase pure WC nanoparticles were successfully synthesized on high surface area Ketjen Black (800 m^2 g^{-1}) by a TPR method. The surface area loss of carbon particles in our process is much smaller compared to other methods since only the carbon atoms on the surface were involved in the process of forming WC using the TPR method. The particle size of WC can be controlled under 30 nm with a relatively good coverage on the carbon surface. The corrosion testing results demonstrated that the corrosion resistance of Ketjen Black was improved by 2-fold with a surface modification by phase pure WC particles. The WC particle itself was not stable during potential cycling. Almost all the WC particles were dissolved or converted to WO*x* after 5000 potential cycles in the potential range of 0.65–1.2 V. However, the test in $HClO_4$ may affect the formation of the WO*x* layer since the acid can leach Cl^- during potential cycling.

The Pt catalysts supported on WC/KB show a similar or slightly better ORR activity compared to that of Pt/KB. The Pt activity loss rate of Pt/WC/KB was slightly lower than that of Pt/KB in the liquid cell testing due to the larger Pt particle size and/or some interaction between Pt and WC. The fuel cell testing results did not reveal a positive effect from WC on durability during potential cycling or potential hold, which may be caused by the change of electrode properties with the formation of WO*x*. Future work will focus on further improvement of the WC deposition on carbon black to fabricate a more uniform WC coating, optimization of the fuel cell

electrode structure, and understanding of the behavior of WC in the fuel cell environment.

Acknowledgements

The work at the NSLS was supported by the DOE BES grant DE-FG02-03ER15688. The synthesis of WC was partially sponsored by the DOE BES grant DE-AC05-76RL01830. We thank Marianne Pemberton and Jonathan Odell for carrying out some experiments.

References

[1] K. Sasaki, M.H. Shao, R.R. Adzic, in: F.N. Buchi, M. Inaba, J. Schmidt (Eds.), Proton Exchange Membrane Fuel Cell Durability, Springer, New York, 2009, pp. 7–28.
[2] K. Kinoshita, Carbon: Electrochemical and Physicochemical Properties, John Wiley & Sons, New York, 1988.
[3] M.F. Mathias, R. Makharia, H.A. Gasteiger, J.J. Conley, T.J. Fuller, C.J. Gittleman, S.S. Kocha, D.P. Miller, C.K. Mittelsteadt, T. Xie, S.G. Yan, P.T. Yu, Interface 14 (2005) 24.
[4] T.F. Fuller, G. Gray, ECS Trans. 1 (2006) 345.
[5] L.M. Roen, C.H. Paik, T.D. Jarvi, Electrochem. Solid-State Lett. 7 (1) (2004) A19–A24.
[6] C.A. Reiser, L. Bregoli, T.W. Patterson, J.S. Yi, J.D. Yang, M.L. Perry, T.D. Jarvi, Electrochem. Solid-State Lett. 8 (6) (2005) A273–A276.
[7] H. Tang, Z.G. Qi, M. Ramani, J.F. Elter, J. Power Sources 158 (2006) 1306.
[8] H. Chhina, S. Campbell, O. Kesler, J. Power Sources 179 (1) (2008) 50–59.
[9] H.H. Hwu, J.G. Chen, Chem. Rev. 105 (2005) 185–212.
[10] A. Serov, C. Kwak, Appl. Catal. B 90 (2009) 313–320.
[11] E.C. Weigert, A.L. Stottlemyer, M.B. Zellner, J.G. Chen, J. Phys. Chem. C 111 (2007) 14617–14620.
[12] H. Chhina, S. Campbell, O. Kesler, J. Power Sources 164 (2) (2007) 431–440.
[13] L.G.R.A. Santos, K.S. Freitas, E.A. Ticianelli, J. Solid State Electrochem. 11 (2007) 1541–1548.
[14] Y. Wang, S. Song, V. Maragou, P.K. Shen, P. Tsiakaras, Appl. Catal. B: Environ. 89 (1–2) (2009) 223–228.
[15] Y. Wang, S. Song, P.K. Shen, C. Guo, C.M. Li, J. Mater. Chem. 19 (2009) 6149–6153.
[16] Y. Wang, DOE Hydrogen and Vehicle Technologies Annual Review, Arlington, 2009.
[17] M.B. Zellner, J.G. Chen, Catal. Today 99 (2005) 299–305.
[18] S. Opalka, M. Belabbes, M.H. Shao, 139th TMS Meeting, Seattle, 2010.
[19] H. Meng, P.K. Shen, J. Phys. Chem. B 109 (48) (2005) 22705–22709.
[20] M. Nie, P.K. Shen, Z. Wei, J. Power Sources 167 (1) (2007) 69–73.
[21] H. Meng, P.K. Shen, Electrochem. Commun. 8 (4) (2006) 588–594.
[22] H. Meng, P.K. Shen, Chem. Commun. (2005) 4408–4410.
[23] E.C. Weigert, M.P. Humbert, Z.J. Mellinger, Q. Ren, J.T.P. Beebe, L. Bao, J.G. Chen, J. Vacuum Sci. Technol. A26 (2008) 23–28.
[24] J.F. Moulder, W.F. Stickle, P.E. Sobol, K.D. Bomben, Handbook of X-ray Photoelectron Spectroscopy, Physical Electronics Inc., Eden Prairie, 1995.
[25] E.C. Weigert, D.V. Esposito, J.G. Chen, J. Power Sources 193 (2009) 501–506.
[26] K.J.J. Mayrhofer, J.C. Meier, S.J. Ashton, G.K.H. Wiberg, F. Kraus, M. Hanzlik, M. Arenz, Electrochem. Commun. 10 (8) (2008) 1144–1147.
[27] T. Ioroi, H. Senoh, S. Yamazaki, Z. Siroma, N. Fujowara, K. Yasuda, J. Electrochem. Soc. 155 (2008) B321–B326.
[28] H. Chhina, S. Campbell, O. Kesler, J. Power Sources 161 (2) (2006) 893–900.
[29] D.A. Stevens, J.R. Dahn, Carbon 43 (2005) 179.
[30] L. Guo, V.M. Swope, B. Merzougui, L. Protsailo, M. Shao, Q. Yuan, G.M. Swain, J. Electrochem. Soc. 157 (1) (2010) A19–A25.
[31] J. Shim, C.-R. Lee, H.-K. Lee, J.-S. Lee, E.J. Cairns, J. Power Sources 102 (1–2) (2001) 172–177.
[32] P. Trogadas, V. Rammani, J. Electrochem. Soc. 70 (2008) B696–B703.
[33] P. Ganesan, S. Huang, B. Popov, ECS Trans. 16 (2008) 1143–1150.